

Supporting Information

Two is not always better than one: ligand optimisation for long-living light emitting electrochemical cells

Rubén D. Costa,^a Enrique Ortí,^a Henk J. Bolink,^{*a} Stefan Graber,^b Catherine E. Housecroft,^b Markus Neuburger,^b and Edwin C. Constable.^{*b}

Materials and Methods. The solvents (puriss grade) were purchased from Fluka. 2-Phenylpyridine and hydrated iridium trichloride were used as received from Aldrich and Johnson Matthey, respectively. UV-vis spectra were recorded in a 1 cm path length quartz cell on a on a 845x UV-visible Agilent spectrophotometer, operating with UV-visible ChemStation Software, Shimadzu UV-3101PC UV/VIS/NIR, or Varian 5000 UV-VIS-NIR spectrophotometers. Steady-state fluorescence spectra were measured on a Photon Technology spectrofluorometer, equipped with a lamp power supply (LPS-220B), working at room temperature. The excited state lifetimes were measured from fresh solutions, which were degassed by Ar bubbling for 30 min. They were deduced from time-resolved absorption spectroscopy utilising a laser flash-photolysis system based on a pulsed Nd:YAG laser, using 355 nm as exciting wavelength. The single pulses were approximately 10 ns duration and the energy was approximately 15 mJ/pulse. A Lo255 Oriel xenon lamp was employed as the detecting light source. The laser flash-photolysis apparatus consisted of the pulsed laser, the Xe lamp, a 77200 Oriel monochromator, and an Oriel photomultiplier (PMT) system made up of 77348 PMT power supply. The oscilloscope was a TDS-640A Tektronix. The output signal from the oscilloscope was transferred to a personal computer.

The quantum yield measurements were performed in a nitrogen environment and determined on a acetonitrile solution of the $[\text{Ir}(\text{ppy})_2(\text{dpbpy})][\text{PF}_6]$ complex using the

quantum yield measurement system from Hamamatsu, model C9920-01. Voltammetric measurements employed a PC-controlled AutoLab PSTAT10 electrochemical workstation. Cyclic voltammograms (CV) were obtained at a scan rate of 100 mV s⁻¹ using 0.1 M TBAPF₆ as supporting electrolyte in acetonitrile. Glassy carbon, sputtered platinum, and platinum wire were employed as working, counter, and reference electrodes, respectively. At the end of each measurement, the ferrocene/ferrocinium (Fc⁺/Fc) potential was measured and used as an internal reference. NMR spectra were measured on a Bruker AM 250 MHz, AV 400 MHz, Bruker DRX-500 MHz, or Bruker Avance 600 MHz spectrometers and the reported chemical shifts are referenced to TMS.

Synthesis and Characterization.

A yellow suspension of tetrakis(2-phenylpyridine-*C,N*)di(μ -chloro)diiridium(III) (350 mg, 0.326 mmol, 1.00 eq) and 6,6'-diphenyl-2,2'-bipyridine (203 mg, 0.659 mmol, 2.02 eq) in MeOH (35 ml) and CH₂Cl₂ (35 ml) was refluxed under an inert atmosphere of N₂ in the dark for 36 h. Silver(I) hexafluorophosphate (167 mg, 0.659 mmol, 2.02 eq) was added to the mixture which was then refluxed for another 20 h. The yellow suspension was then cooled down to room temperature, and solid ammonium hexafluorophosphate (532 mg, 3.26 mmol, 10.0 eq) was added to the solution. The mixture was stirred for 1 h at room temperature and then evaporated to dryness. The crude material was purified on Alox (Merck Alox 90, CH₂Cl₂ → CH₂Cl₂:MeOH = 100:1) yielding the desired product as an orange solid (554 mg, 0.581 mmol, 89 %).

mp 195 – 200 °C.

MS (ESI, *m/z*): 809.2 [M-PF₆]⁺ (calc. 809.2); 501.1 [M-dpbpy-PF₆]⁺ (calc. 501.1).

Calcd. for C₄₄H₃₂F₆IrN₄P·0.5H₂O (962.94)

C 54.88, H 3.45, N 5.82; found C 54.82, H 3.36, N 5.80 %.

UV-Vis λ / nm (ϵ / $\text{l}\cdot\text{mol}^{-1}\text{cm}^{-1}$) (CH_2Cl_2 , $9.99\text{E-}6$ $\text{mol}\cdot\text{l}^{-1}$) 267 (43 000), 311 (sh, 27 000);
(CH_2Cl_2 , $9.99\text{E-}5$ $\text{mol}\cdot\text{l}^{-1}$) 383 (sh, 5 200); (CH_2Cl_2 , $4.00\text{E-}4$ $\text{mol}\cdot\text{l}^{-1}$) 474 (920).

Fluorescence (CH_2Cl_2 , $c = 9.99\text{E-}6$ $\text{mol}\cdot\text{l}^{-1}$, $\lambda_{\text{ex}} = 316$ nm): $\lambda_{\text{em}} = 579$ nm; lifetime $\tau = 98$ ns ($\chi^2 = 1.050$).

IR (neat): $\nu = 3045$ (w), 2627 (w), 1983 (w), 1607 (m), 1585 (m), 1564 (m), 1477 (m), 1452 (m), 1421 (m), 1307 (w), 1271 (w), 1229 (w), 1163 (w), 1128 (w), 1063 (w), 1030 (w), 1003 (w), 827 (s), 752 (s), 729 (s), 694 (s) cm^{-1} .

^1H NMR (500 MHz, CD_2Cl_2) δ / ppm 8.42 (d, $^3J = 8.0$ Hz, 2H, $\text{H}^{3(\text{A})}$), 8.26 (d, $^3J = 5.7$ Hz, 2H, $\text{H}^{6(\text{C})}$), 8.15 (t, $^3J = 7.9$ Hz, 2H, $\text{H}^{4(\text{A})}$), 7.83 (t, $^3J = 7.8$ Hz, 2H, $\text{H}^{4(\text{C})}$), 7.65 (d, $^3J = 8.2$ Hz, 2H, $\text{H}^{3(\text{C})}$), 7.34 (d, $^3J = 7.7$ Hz, 2H, $\text{H}^{5(\text{A})}$), 7.16 (t, $^3J = 6.6$ Hz, 2H, $\text{H}^{5(\text{C})}$), 7.11 (d, $^3J = 7.8$ Hz, 2H, $\text{H}^{6(\text{D})}$), 7.01 (t, $^3J = 7.5$ Hz, 2H, $\text{H}^{4(\text{B})}$), 6.76 (t, $^3J = 7.8$ Hz, 4H, $\text{H}^{3(\text{B})}$), 6.60 (d, $^3J = 6.2$ Hz, 4H, $\text{H}^{2(\text{B})}$), 6.55 (t, $^3J = 7.5$ Hz, 2H, $\text{H}^{5(\text{D})}$), 6.21 (t, $^3J = 7.5$ Hz, 2H, $\text{H}^{4(\text{D})}$), 5.24 (d, $^3J = 7.8$ Hz, 2H, $\text{H}^{3(\text{D})}$).

^{13}C NMR (126 MHz, CD_2Cl_2) δ / ppm 168.33 ($\text{C}^{2(\text{C})}$), 165.56 ($\text{C}^{6(\text{A})}$), 159.38 ($\text{C}^{2(\text{A})}$), 150.37 ($\text{C}^{6(\text{C})}$), 146.81 ($\text{C}^{2(\text{D})}$), 141.85 ($\text{C}^{1(\text{D})}$), 139.68 ($\text{C}^{4(\text{A})}$), 138.41 ($\text{C}^{1(\text{B})}$), 138.35 ($\text{C}^{4(\text{C})}$), 131.09 ($\text{C}^{3(\text{D})}$), 130.01 ($\text{C}^{5(\text{A})}/\text{C}^{4(\text{D})}$), 129.98 ($\text{C}^{5(\text{A})}/\text{C}^{4(\text{D})}$), 128.72 ($\text{C}^{4(\text{B})}$), 128.02 ($\text{C}^{3(\text{B})}$), 127.51 ($\text{C}^{2(\text{B})}$), 124.63 ($\text{C}^{3(\text{A})}$), 124.42 ($\text{C}^{6(\text{D})}$), 122.37 ($\text{C}^{5(\text{C})}$), 121.25 ($\text{C}^{5(\text{D})}$), 119.75 ($\text{C}^{3(\text{C})}$).

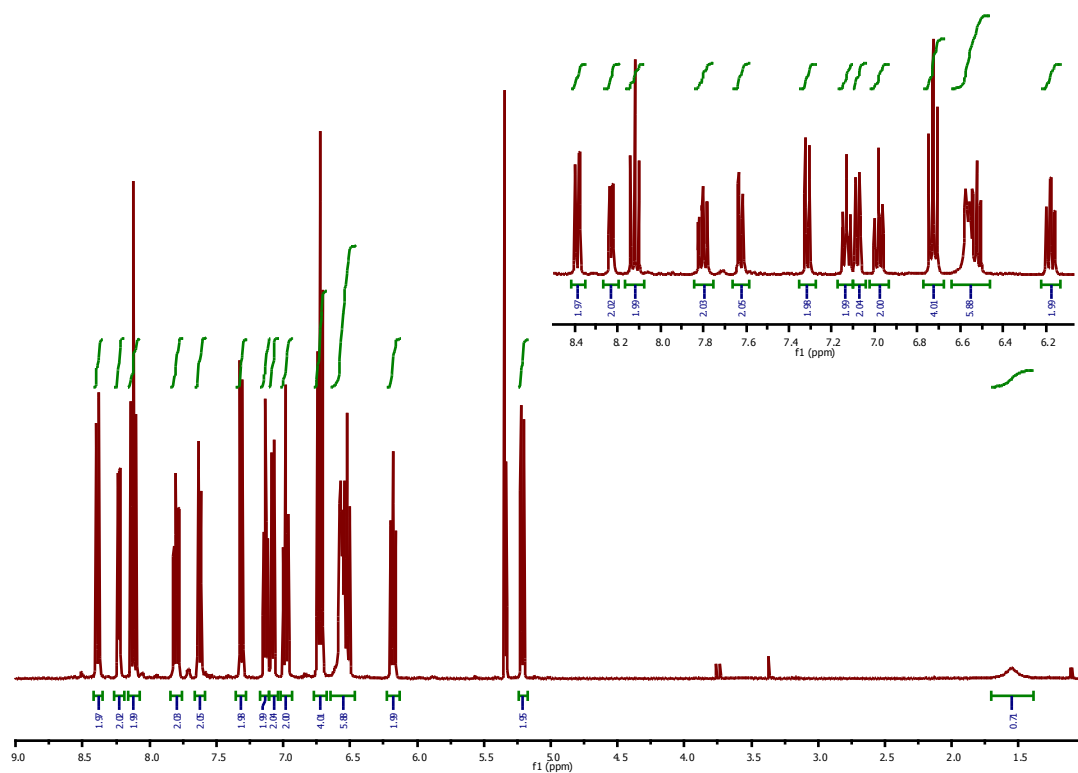


Figure S1. ^1H NMR spectrum of $[\text{Ir}(\text{ppy})_2(\text{dpbbp})][\text{PF}_6]$ in CD_2Cl_2 and expansion of the aromatic region of the spectra.

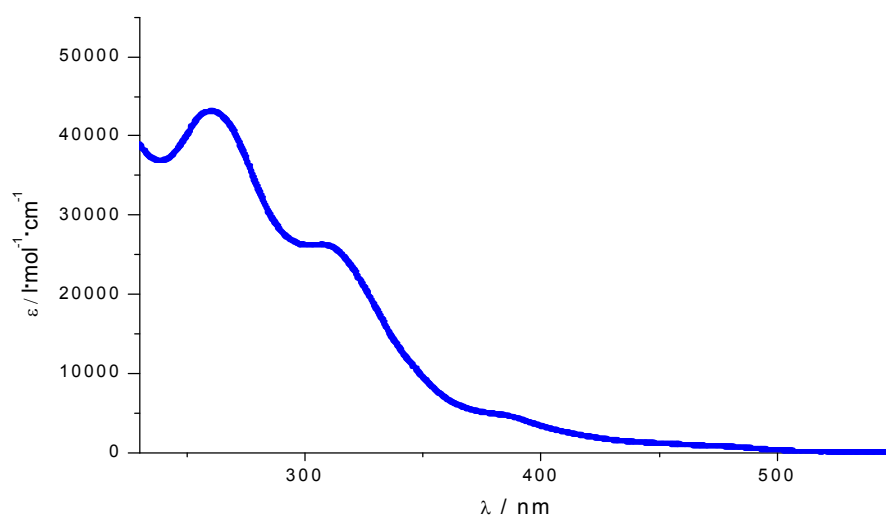


Figure S2. Absorption spectra of $[\text{Ir}(\text{ppy})_2(\text{dpbpy})][\text{PF}_6]$ in acetonitrile solution.

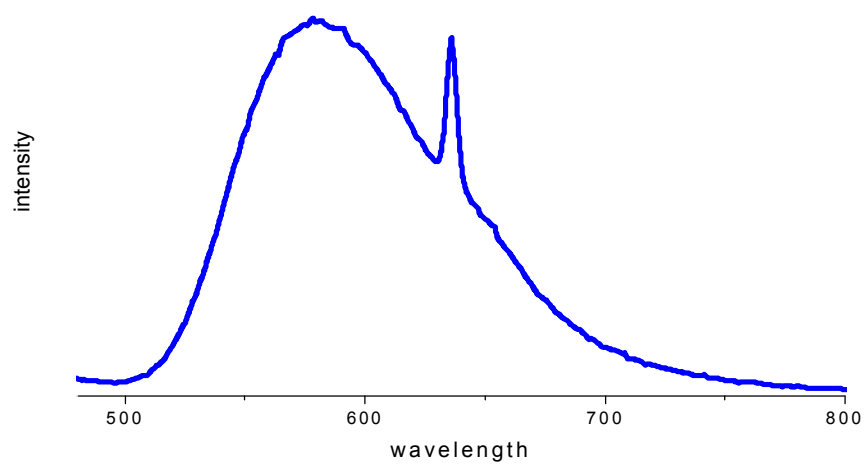


Figure S3. Emission spectra of $[\text{Ir}(\text{ppy})_2(\text{dpby})][\text{PF}_6]$ in dichloromethane solution.

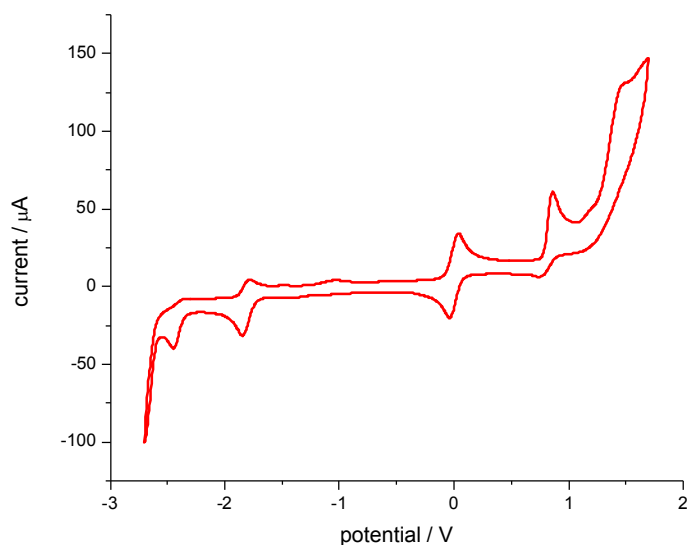


Figure S4. Cyclic voltammometry data of $[\text{Ir}(\text{ppy})_2(\text{dpby})][\text{PF}_6]$ in acetonitrile solution containing 0.1M $[\text{nBu}_4\text{N}][\text{PF}_6]$ as supporting electrolyte, internal reference Fc/Fc^+ .

Computational Details. Density functional calculations (DFT) were carried out with the C.02 revision of the Gaussian 03 program package,^[1] using Becke's three-parameter B3LYP exchange-correlation functional^[2-4] together with the 6-31G** basis set for C, H, and N atoms^[5] and the “double- ζ ” quality LANL2DZ basis set for the Ir element.^[6] An effective core potential (ECP) replaces the inner core electrons of Ir leaving the outer core $[(5s)^2(5p)^6]$ electrons and the $(5d)^6$ valence electrons of Ir(III). The geometries of the singlet ground state (S_0) and of the triplet excited states T and ^3MC (d-d) of $[\text{Ir}(\text{ppy})_2(\text{pbpy})]^+$ and $[\text{Ir}(\text{ppy})_2(\text{dpby})]^+$ were fully optimized without symmetry restrictions. Triplet states were calculated at the spin-unrestricted UB3LYP level with a spin multiplicity of 3. The expected values calculated for S^2 were always smaller than 2.05.

The minimum-energy optimized geometry calculated for the S_0 state of both complexes (Figure S5) shows the intramolecular π - π interaction observed in the solid state between the pendant phenyl rings of the bpy ligand with the adjacent ppy ligands. Calculations predict that the intramolecular π - π interaction is preserved for the lowest triplet excited state. This makes the complex more robust in the excited emitting state and reduces the possibility for ligand-exchange reactions leading to the degradation of the complex.

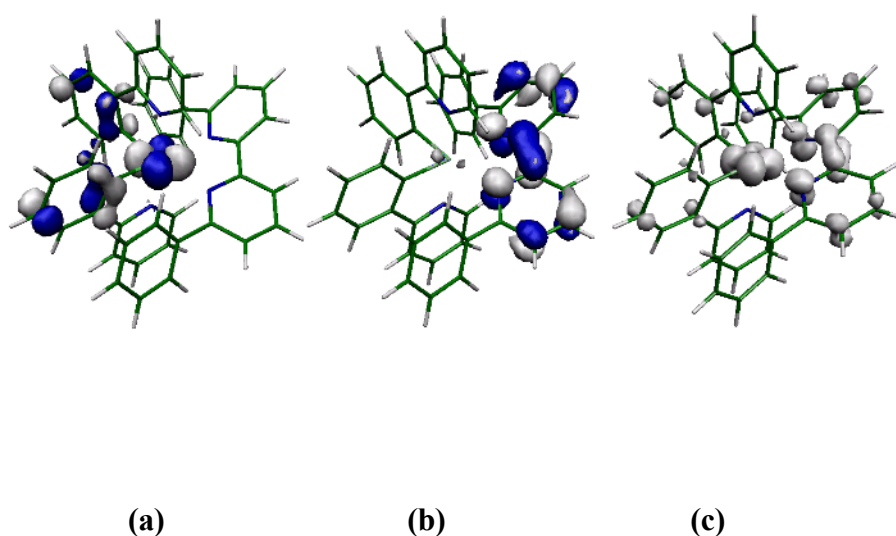


Figure S5. Electronic density contours (0.06 e bohr^{-3}) calculated for the HOMO (a) and LUMO (b) of the $[\text{Ir}(\text{ppy})_2(\text{dpbbpy})]^+$ complex in its S_0 ground state. (c) Spin density distribution ($0.006 \text{ e bohr}^{-3}$) calculated for $[\text{Ir}(\text{ppy})_2(\text{dpbbpy})]^+$ in the T excited state.

As depicted in Figure S5, the highest occupied molecular orbital (HOMO) is composed of a mixture of Ir d_π orbitals ($\approx 48\%$) and phenyl π orbitals distributed mainly in one ppy ligand in both complexes. The lowest unoccupied molecular orbital (LUMO) resides on the diimine N^N ligand in both complexes and shows no overlap with the HOMO. The emissive T state originates from the HOMO \rightarrow LUMO excitation

implying an electron transfer from the Ir-ppy environment to the pbpy or dpbpy and is located 2.22 eV ($[\text{Ir}(\text{ppy})_2(\text{pbpy})]^+$) and 2.32 eV ($[\text{Ir}(\text{ppy})_2(\text{dpbpy})]^+$) above the S_0 state (adiabatic energy difference). The nature of T should be therefore described as a mixture of metal-to-ligand and ligand-to-ligand charge transfer ($^3\text{MLCT}$ and $^3\text{LLCT}$, respectively) due to the participation of both the Ir atom and the phenyl rings of the ppys in the HOMO (see Figure S5). The spin densities calculated for the optimized geometry of T are [Ir: 0.52, ppy: 0.25 and 0.12, pbpy: 1.10] for the ($[\text{Ir}(\text{ppy})_2(\text{pbpy})]^+$) complex and [Ir: 0.50, ppy: 0.18 and 0.19, dpbpy: 1.13] for the ($[\text{Ir}(\text{ppy})_2(\text{dpbpy})]^+$) confirms the mixed $^3\text{MLCT}$ – $^3\text{LLCT}$ character of this state. The CT nature of the emitting state is in agreement with the broad and unstructured aspect of the emission band observed at $\lambda_{\text{max}} = 595$ nm for both complexes (Figure S3). To estimate the phosphorescence emission energy, the vertical energy difference between T and S_0 was computed by performing a single-point calculation of S_0 at the optimized minimum-energy geometry of T. Calculations lead to a vertical emission of 2.02 eV for the ($[\text{Ir}(\text{ppy})_2(\text{dpbpy})]^+$) in a good agreement with the experimental value for the maximum emission (2.08 eV).

Table S1. Calculated values for selected bond distances (in Å) of ($[\text{Ir}(\text{ppy})_2(\text{pbpy})]^+$) and ($[\text{Ir}(\text{ppy})_2(\text{dpbpy})]^+$) in the S_0 singlet ground state and in the T and ^3MC triplet excited states

	$[\text{Ir}(\text{ppy})_2(\text{pbpy})]^+$		
	S_0	T	^3MC
ppy			
Ir-C	2.012	2.019	2.021
Ir-N	2.093	2.086	2.577
ppy π-π interaction			

Ir-C	2.027	1.986	2.021
Ir-N	2.079	2.074	2.239
bpy			
Ir-N _{phen}	2.375	2.227	2.474
Ir-N	2.217	2.225	2.250
[Ir(ppy)₂(dpbpy)]⁺			
ppy			
Ir-C	2.020/2.019	2.008/1.996	2.047/2.025
Ir-N	2.081/ 2.077	2.077/2.074	2.201/2.578
bpy			
Ir-N	2.360/2.367	2.275/2.293	2.324/2.534

³MC states were computed starting from the optimized geometry of S₀ with Ir-N_{ppy} bond distances lengthened to 2.70 Å. The geometries structures of ³MC states in both complexes are similar (See Table S1). The spin densities calculated for the optimized geometries corroborate the metal-centered character of the triplet state converged both for [Ir(ppy)₂(pbpy)]⁺ and for [Ir(ppy)₂(dpbpy)]⁺. As shown in Figure S6, the spin densities are mainly concentrated on the metal, which holds 1.53 and 1.49 unpaired electrons, respectively, and reflect the interactions along the N–Ir–N axis. The ³MC state is calculated to be above the lowest-energy T state by 0.65 eV for [Ir(ppy)₂(pbpy)]⁺ and by 0.26 eV for [Ir(ppy)₂(dpbpy)]⁺ (adiabatic energy differences).

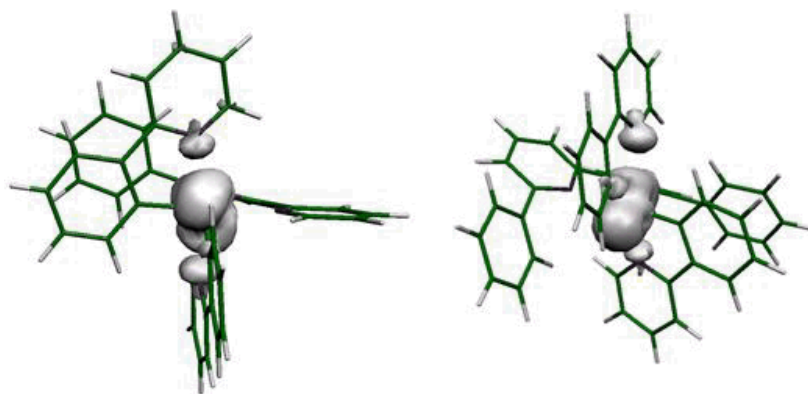


Figure S6. Spin densities calculated for the optimized ^3MC states of $[\text{Ir}(\text{ppy})_2(\text{pbpy})]^+$ (left) and $[\text{Ir}(\text{ppy})_2(\text{dpbpy})]^+$ (right).

Device Preparation and Characterization. Poly(3,4-ethylenedioxythiophene):polystyrenesulfonate (PEDOT:PSS) was purchased from HC-Starck and solvents used were obtained from Aldrich. Indium tin oxide (ITO)-coated glass plates ($15 \Omega^{-1}$) were patterned using conventional photolithography (obtained from Naranjosubstrates, www.naranjosubstrates.com). The substrates were extensively cleaned using sonification in subsequently water-soap, water, and 2-propanol baths. After drying, the substrates were placed in a UV-ozone cleaner (Jelight 42-220) for 20 minutes.

The electroluminescent devices were prepared as follows. Transparent thin films of the $[\text{Ir}(\text{ppy})_2(\text{pbpy})][\text{PF}_6]$ and $[\text{Ir}(\text{ppy})_2(\text{dpbpy})][\text{PF}_6]$ complexes containing different amount of the ionic liquid (1-butyl-3-methylimidazolium hexafluorophosphate) were

obtained by spinning from acetonitrile solutions using concentrations of 20 mg mL⁻¹ at 2000 rpm for 40 seconds, resulting in a 90 nm thick film. Prior to the deposition of the emitting layer a 100 nm layer of PEDOT:PSS was deposited to increase the device preparation yield. The thickness of the films was determined using an Ambios XP1 profilometer. After spinning the organic layers, the samples were transferred to an inert atmosphere glovebox (< 0.1 ppm O₂ and H₂O, MBraun) and dried on a hot plate at 80 °C for 1 hour. Aluminium metal electrodes (80 nm) were thermally evaporated using a shadow mask under a vacuum (< 1×10⁻⁶ mbar) using an Edwards Auto500 evaporator integrated into an inert atmosphere glovebox.

Current density and luminance versus voltage were measured using a Keithley 2400 source meter and a photodiode coupled to a Keithley 6485 pico-amperometer using a Minolta LS100 to calibrate the photocurrent. External quantum efficiencies (EQE) were determined using an integrated sphere coupled to an UDT instruments S370 Optometer. An Avantes luminance spectrometer was used to measure the EL spectrum. Lifetime data were obtained by applying a constant voltage over the device and monitoring the current flow and simultaneously the current generated by a Si-photodiode (Hamamatsu S1336-8BK) calibrated using a Minolta LS100 luminance meter. Custom-made equipment consisting of a multi-channel rack, from muetta consult, 16 boards with power source, and DAQ (data acquisition)-12 bits ADC (analogue to digital converter). A custom-designed labview program was used to control the equipment and gather the data on a personal computer. Both the multi-channel rack and the PC are connected via an autonomic power supply unit (SALICRU SLC cube).

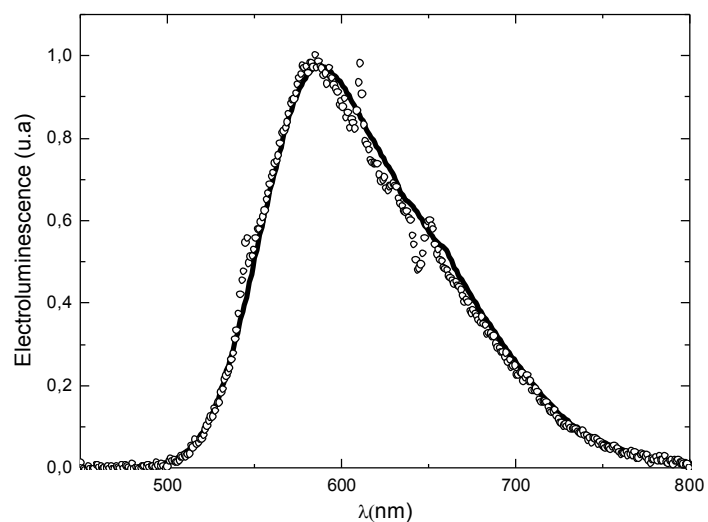


Figure S7. Electroluminescence spectrum of the ITO/PEDOT:PSS/[Ir(ppy)₂dpby]:IL (4:1)/Al (open circle) and ITO/PEDOT:PSS/[Ir(ppy)₂pbpy]:IL(4:1)/Al (solid line) device at 3V.

References

- 1 M. J. T. Frisch *et al.*, Gaussian 2003, Revision C.02 (Gaussian Inc.: Pittsburgh PA, 2003).
- 2 A. D. Becke, *J. Chem. Phys.*, 1988, **88**, 2547.

3 A. D. Becke, *J. Chem. Phys.*, 1993, **98**, 5648.

4 C. T. Lee, W. T. Yang, R. G. Parr, *Phys. Rev.*, 1988, **37**, 785.

5 M. M. Francl, W. J. Pietro, W. J. Hehre, J. S. Binkley, M. S. Gordon, D. J. Defrees, J.

A. Pople, *J. Chem. Phys.*, 1982, **77**, 3654.

6 P. J. Hay, W. R. Wadt, *J. Chem. Phys.*, 1985, **82**, 299.